ELSEVIER

Journal of Molecular Catalysis A: Chemical 127 (1997) 163–190

JOURNAL OF MOLECULAR CATALYSIS A: CHEMICAL

Modelling of hydrotreating catalysis based on the remote control: HYD and HDS

Y.W. Li [1], B. Delmon *

Groupe de Physico-Chimie Minérale et de Catalyse, Place Croix du Sud 2 / 17, B-1348 Louvain-la-Neuve, Belgium

Received 30 March 1997; accepted 17 May 1997

Abstract

The remote control theory was used to construct a comprehensive kinetic model of hydrodesulfurization (HDS) and hydrogenation (HYD) on sulfided catalysts. The work makes an attempt to reflect in a more precise way the structure of the active sites. By considering available information on the HYD and HDS catalysis over promoted MoS_2 type catalysts, several new kinetic models were developed. They were inserted into a continuous stirred tank reactor (CSTR) model to simulate both the steady states and the dynamic trends of the hydrodesulfurization and hydrogenation of model feeds represented by a mixture of thiophene and unsaturated hydrocarbons. These trends are qualitatively compared with the experimental observations in order to discriminate these slightly different models. It is found that the interconversion of HYD sites to HDS sites necessitates spillover hydrogen rather than the adsorption of hydrogen sulfide. The models based on the remote control are able to predict synergetic behaviors observed in experiments. © 1997 Elsevier Science B.V.

Keywords: Hydrotreating; Remote control; Surface dynamics; Kinetics; Structure of active sites; Simulation

1. Introduction

It has taken a very long time before it was universally recognized that at least two kinds of active sites existed on the hydrotreating catalysts for, respectively, the hydrogenation (HYD) of unsaturated molecules and the hydrodesulfurization (HDS) of sulfur-containing compounds. But the fact that HYD and HDS sites can interconvert into each other when the hydrogen and hydrogen sulfide proportion changes is not yet universally accepted, in spite of strong experimental arguments [1–8]. This interconversion is explained by the remote control theory, which is receiving many confirmations from various sets of experiments [1–3,6]. We recall that, according to this theory, the active sites in HYD and HDS are created by a kind of dissociated species of hydrogen, called spillover hydrogen,

* Corresponding author.

[1] On leave from State-Key Laboratory of Coal Conversion, Institute of Coal Chemistry, Chinese Academy of Sciences, Taiyuan 030001, China.

PII S1381-1169(97)00121-0

H_{so}, flowing from some promoters (donor) of hydrotreating catalysts (namely Co_9S_8 promoted MoS_2 or WS_2) to the active phase (acceptor, usually MoS_2 or sometimes WS_2). This spillover species reacts with the MoS_2 (or WS_2) surface to create HYD and HDS sites.

On the other hand, the hydrotreating of petroleum fractions has become increasingly more sophisticated in the course of years. This results from the necessity to produce fuels meeting the increasingly stringent requirements imposed by environmental regulations (deep dearomatization and deep HDS in particular). Not only new catalysts designed according to modern concepts, but also new process operation procedures will be necessary to economically satisfy these regulations, which seem presently difficult to reach. It becomes clear that the classical Langmuir–Hinshelwood representation is insufficient to describe the hydrotreating kinetics. A modern accurate modelling of hydrotreatment reactions is therefore needed. This should take into account all the specificities of the hydrotreatment reactions. A systematic investigation on the thiophene HDS, at both the kinetic level and the pellet/reactor level, has been reported by Froment and his coworkers [2,9–12]. Especially the recent model of Pille and Froment [2] constituted a considerable advance because it took into account the role of spillover hydrogen H_{so}. But this model considered only steady-state situations and did not take into account all the dynamic aspects, in particular transient situations, due to the fact that, according to the remote control theory, a flux of spillover hydrogen H_{so} must be established between the catalyst promoter and MoS_2 (or WS_2). This flux varies when the experimental conditions change.

We propose here a family of new models, which reflect all the aspects of the remote control theory with emphasis on the particular dynamic process involved in this theory. One of the bases of our approach is the work by Froment and his coworkers [2,9,10,12], which modelled the remote control and site interconversion in hydrotreating, but did not consider the dynamics of the diffusion of H_{so} from the promoter (donor) to the active MoS_2 phase (acceptor) and took only partially into account the structural information concerning catalyst surface and active sites. The other basis is a comprehensive model developed for the remote control in selective oxidation by Rebitzki et al. [13]. Our models combine, in a logical way, all the available information provided both by theory and by experiments, namely the structure of the catalytic surface, the possible structure of the active sites, the probable mechanisms for HYD and HDS, the hydrogen migration from donor (Co_9S_8) to acceptor (MoS_2) and the creation of active sites on MoS_2 by the reaction of spillover hydrogen, $H_{so,Mo}$, having reached the MoS_2 phase, with the edges of MoS_2 slabs. The methodological approach is similar to that proposed by Rebitzki et al. [13] in the case of selective oxidation. We combine the detailed kinetics of all elementary steps, including the migration of H_{so}, into a dynamic continuous stirred tank (CST) reactor model. One of the original features of the work is to simulate both the transient states and the steady states of the catalyst surface and the overall reactor. Engineers working in hydrotreatment know that a catalyst does not immediately reach the steady state activity, neither at the start of the operation nor when the operation conditions and/or the feed are modified.

2. Experimental and theoretical bases

The exact micro-structure of the catalyst surface at atomic/molecular level is not yet fully understood. One of the reasons is that it has not been possible yet to investigate catalysts in the state they are in under the real reaction conditions, namely at high pressure and in the presence of H_2 and H_2S. Even the characterization of catalysts after they have been subjected to realistic reaction conditions seems very difficult [1,6,8].

In spite of this limitation and the consequence that literature is still debating on the nature of the active sites in the promoted MoS_2 catalysts for HDS and HYD, it has generally been agreed that coordinatively unsaturated metal sites (CUS) are essential for the activity in HDS and HYD reactions. There is some agreement that 3-fold CUS sites located at specific crystallographic sites on edges are responsible for the HYD. This is based on the extensive experimental studies of Kasztelan et al. [14,15]. The assumption of 3-fold CUS sites for HYD seems generally adequate on the basis of both geometrical and stoichiometric considerations. There is another general agreement that the HDS sites are also situated on the edges of the MoS_2 (or WS_2) slabs [1,8,14–26]. The situation, however, is more complicated. A correlation of thiophene HDS activity with the S/Mo ratio of catalysts was reported by several authors [16–21], and summarized by Kasztelan et al. [15]. It was found that the HDS activity had a maximum value at S/Mo ratio close to 1, namely corresponding to a highly reduced state of the MoS_2 edges. However, it is difficult to define the composition and coordination of the active sites exactly, because many possibilities exist for structures of the edges of MoS_2 slabs. By taking into account these experimental results [16–21] and that of Kasztelan et al. [14], the structure of HDS sites may compare to highly reduced CUS sites on the edges of MoS_2 slabs, namely a higher coordination unsaturation for HDS than for HYD. Incidentally, this may be related to the fact that the isomerization activity of 4-fold CUS sites is much higher than that of two-fold CUS sites [14]. It should also be noticed that under the high hydrogen pressure normally used in industrial units, more highly reduced sites namely 4-fold CUS sites, could logically exist and constitute the precursors of HDS sites. We use the word *precursors* because these sites may have to be modified further for becoming active; this would occur as a consequence of the presence of both hydrogen and sulfur compounds on the surface under the real operation conditions.

An additional complication is the existence of atomic or protonic hydrogen species and SH groups on the active surface. Besides the CUS sites, these surface species might play a role in hydrotreating reactions (this is strongly suspected for hydrodenitrogenation (HDN)). One reason to consider this possibility is that the exchange of these surface species with bulk molecules has been observed [8,26–29]. This reflects one aspect of the complex and dynamic nature of the HDS and HYD catalyst surface. This complexity suggests that neither the HYD nor the HDS sites can be understood correctly with the conventional viewpoint, namely assuming that the amount of catalytic sites remains identical when the reaction conditions change [2,7,8,24].

A short discussion of the structure of the active phase and the molecular-atomic structure of the active sites in HYD and HDS can help understand why the structure of active sites can change in hydrotreating catalysts. This results from the possibility of changes in coordination of molybdenum atoms located on the edge of MoS_2 slabs when the environment changes. Molybdenum sulfide has a layered structure, in which single layers of Mo^{4+} are sandwiched between two layers of closely packed S^{2-} anions as schematically shown in Fig. 1. In the bulk of the layered structure, each Mo atom is surrounded by six sulfur atoms in a trigonal prismatic coordination, where each sulfur atom is strongly bound to three Mo atoms [30–33]. Eijsbouts and Heinerman investigated the correlation between HDS and HYD activities and MoS_2 dispersion on an Al_2O_3 support [22,23]. The TEM micrographs were used to semi-quantitatively identify the MoS_2 slabs and their dispersion. It was found that MoS_2 slabs on the supports varied from single to 6 layers thick and were mostly from 3.33 to 4.59 nm long. In spite of the unknown structure of the stacks of MoS_2 slabs, many possibilities for the states of the edge metal sites exist for a working MoS_2 slab [22,23]. However, a slab of MoS_2 in real catalysts can schematically be represented by Fig. 1a. Fig. 1b represents a basal plane view of a perfect slab (all Mo atoms are fully coordinated with S atoms). Fig. 1b shows that there are two types of edges, oriented in the directions $(\bar{1}010)$ and $(10\bar{1}0)$. These, viewed laterally, are schematically

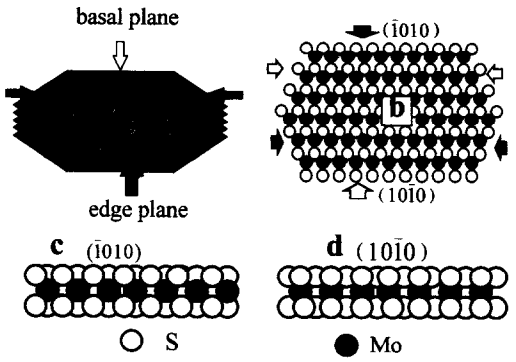

Fig. 1. MoS_2 slabs and their edges. (a) A perfect real slab, (b) basal plane view of a perfect slab, (c) view of $(\bar{1}010)$ edge and (d) view of $(10\bar{1}0)$ edge.

shown in Fig. 1c and d, respectively. The sulfur atoms existing in a perfect slab may be classified, according to their coordination states, into three types, namely terminal ones, S(T), bridging ones, S(B) and basal plane ones, S(S), each of which is strongly bonded to three Mo atoms.

The reactivity of these S atoms with hydrogen determines the possibility of reducing the surface of MoS_2 slabs, namely the activation of the catalysts. This has been comprehensively discussed by Yermakov et al. [34]. They considered the removal of S atoms through a reaction of different types of S atoms with hydrogen as follows:

$$M\text{-}S + H_2 \rightarrow M\text{-}\otimes + H_2S$$

where M represents a metal center, which may have different configurations, S the sulfur atom, which may be terminal S(T), bridging S(B), or situated on a basal plane S(S) and $\otimes$ a vacancy formed on the M site by removing one such S atom. The enthalpies of the above reactions were calculated as the difference of the sums of atomization enthalpies of the products and initial reagents for different kinds of S atoms. The results can be summarized as follows: -25 kcal/mol $< \Delta H_{S(T)} < -5$ kcal/mol, $\Delta H_{S(B)} \approx 21.5$ kcal/mol and $\Delta H_{S(S)} \approx 82.3$ kcal/mol. The atomization enthalpies were calculated by using a semi-empirical approach (IBM technique) [34]. These results indicate that under the hydrogen atmosphere the removal of S(T) atoms leads to a decrease of the total energy of the system making it more stable, while the removal of S(B) atoms leads to a considerable increase and S(S) atoms to a substantial increase of the total energy.

Therefore, it is reasonable to assume that S(T) atoms will not remain on the $(10\bar{1}0)$ edges any more as soon as the working conditions start being established, leaving Mo sites with 2-fold CUS on these $(10\bar{1}0)$ edges. In fact, 2-fold CUS is the highest level to which $(10\bar{1}0)$ edges can get reduced because it is impossible to remove S(S) atoms vicinal to $(10\bar{1}0)$ Mo atoms under typical hydrotreating conditions. If HYD and HDS activities are considered, the $(10\bar{1}0)$ edges must be inactive because the corresponding sites are expected to be in a higher reduction state [14–21]. On $(\bar{1}010)$ edges, however, each Mo atom is bonded with 4 S(B) atoms and 2 S(S) atoms (Fig. 1b and c). The S(B) atoms can be removed in hydrotreating provided the H_2/H_2S ratio is sufficient because of their moderate binding energies. This can be greatly facilitated by mobile hydrogen atoms/protons [30], defined by the remote control theory as spillover H_{so}, available on the catalyst surface because H_{so} consistently exhibits very high reactivities in all other phenomena it brings about [35]. The reduction of $(\bar{1}010)$ edges leads to several possible types of sites as shown in Fig. 2. The removal of S(B) atoms may lead to vacancies from 1-fold CUS to maximum 4-fold CUS sites. For 4-fold CUS sites, each Mo atom

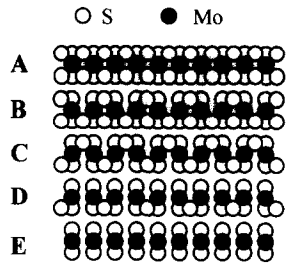

Fig. 2. ($\bar{1}010$) edges with different reduction extents. (A) Perfect edge with full coordinated Mo atoms, (B) I-CUS edge, (C) 2-CUS edge, (D) 3-CUS edge and (E) 4-CUS edge (maximum).

bonds to 2 S(S) atoms. Removal of these S(S) atoms would be possible only in extreme conditions (very high temperature) because of the strong binding energy, and this would destroy the structure of MoS_2. When considering Fig. 2, one assumption may be made on the basis of the fact that the removal of S(B) atoms to form 3-fold CUS sites, namely the ones responsible for HYD [14,15], is more difficult than the removal of those to form 1 or 2-fold CUS sites. The work will therefore focus on the formation of 3-fold CUS sites from the 2-fold CUS ones and this transformation in the kinetic models. We assume that 3-fold CUS sites are formed from 2-fold CUS ones and this step is kinetically important. This leads to assuming that the 2-fold CUS ($\bar{1}010$) edges may be considered as existing on the initial active surface. Fig. 3, a schematic view of an edge surface from a direction perpendicular to the basal plane, suggests how sulfur atoms can be removed by hydrogenolysis of Mo–S bonds, making 3-fold CUS sites out of 2-fold ones on the edges.

The 3-fold CUS sites can also be further modified to form HDS sites [1,6,36]. If we accept the fact that the structure and coordination of sites can change, it is easy to understand the mechanism by which active sites form or change. Sulfhydryl groups mentioned by some authors [1,8,27–29,36] can develop by the opening of a Mo–S–Mo bridge with hydrogen and, together with 3-fold CUS sites, form HDS sites. An alternative picture can be proposed according to the models we shall develop, which supposes that atomic hydrogen, in the form of spillover species $H_{so,Mo}$ moving on MoS_2 can remove a sufficient number of edge sulfur atoms (S(B) on ($\bar{1}010$) edges) and open an Mo–S–Mo bridge to create SH groups, thus keeping the surface in the reduced state required for the formation of active sites. The theory proposes more precisely that $H_{so,Mo}$ maintains an adequate balance between sulfurization and reduction of the MoS_2 phase.

Promoters of MoS_2 catalysts, like Co_9S_8 and Ni_xS_y, can enhance the supply of the atomic hydrogen [30], and the equilibrium can then be displaced in the direction of more reduced (3-fold and -SH modified) sites on the surface. This picture corresponds to the remote control theory [1]. With respect to the HDS sites, several possibilities exist, between which no discrimination is possible on the basis of existing results. These possibilities are: (1) more reduced sites, namely 4-fold coordination unsaturated Mo atoms (Fig. 4A, two sites represented), (2) a sort of composite site constituted of two 3-CUS sites, one carrying an SH group and another carrying a proton, both formed by the action of $H_{so,Mo}$ as shown in Fig. 4B (one HDS site) and (3) single 3-fold Mo sites with vicinal SH groups,

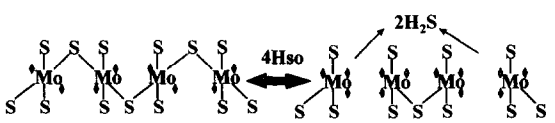

Fig. 3. Schematic representation of inactive edge sites (2-CUS's on ($\bar{1}010$)) to HYD sites.

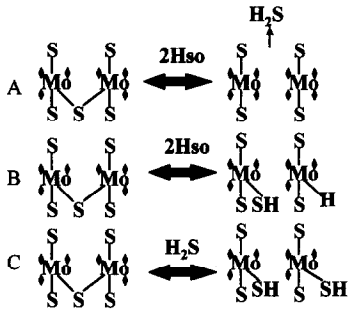

Fig. 4. Possibilities of the interconversion between HYD and HDS sites.

formed by dissociated adsorption of H_2S as shown in Fig. 4C (two HDS sites). It should however be underlined that not all the possibilities are covered by the above. The essential aspect of the above presentation is to show that site interconversion is possible through the action of species, like H_2S and $H_{so,Mo}$. The above discussion emphasizes the role of the atomic hydrogen species, namely spillover H_{so} [1]. This is not in contradiction with the interpretation of Li et al. [30]. These authors suggested that the enhancement of the HYD and HDS activity by adding a promoter in MoS_2 type catalysts could be ascribed to the enhancement of hydrogen dissociation. This is in essence similar to the hypothesis on which the remote control mechanism is based. But the remote control theory is more precise in that it supposes that dissociated hydrogen atoms are formed on the promoter (Co_9S_8, Ni_xS_y) and migrate from this promoter to the active phase, namely MoS_2, where it is consumed. The consequent dynamic picture is that the surface diffusion of atomic hydrogen controls the balance of supply and consumption of hydrogen between the promoter and the active phase of HDS and HYD.

But it should not be forgotten that experiments show that the MoS_2 catalysts without any promoter have a significant activity for HDS and HYD. This can be explained by the defective structure of MoS_2 slabs, namely the fact that some sites normally possess 3 or 4-fold vacancies because the structure of MoS_2 makes that the edges of MoS_2 slabs are 'rough' at the atomic scale, especially at the intersection of edges corresponding to different orientations. These sites are structure dependent, and they are probably modified by H_2S as considered in the present kinetic models based on the kinetic analysis of HDS and HYD reactions [2,7,37].

An additional complication of the mechanism is the possibility that the promoter, e.g. Co_9S_8, can itself undergo a reduction by hydrogen in reaction conditions when too little or no H_2S is present and consequently lose its ability to produce spillover hydrogen [12,38]. This possibility seems necessary to explain some special phenomena, but strong evidence of its occurrence in usual HDS and HYD conditions is still lacking.

3. Modelization of the mechanism

3.1. Spillover process

The first steps to consider for the modelization of the HDS and HYD catalysis mechanism are those accounting for the production of mobile hydrogen, namely spillover H_{so}, on the promoter, the transfer of this hydrogen from the promoter (donor) to the active phase (acceptor) and the creation of

the active sites on the active phase. The generation of spillover hydrogen on the donor, Co_9S_8, can be described as follows:

$$2Co + H_2 \leftrightarrow 2HCo \tag{S1}$$

$$HCo \leftrightarrow Co + H_{so,Co} \tag{S2}$$

$$2Co + 2H_{so,Co} \leftrightarrow 2Co_r + H_2S \tag{S3}$$

The symbol Co does not imply any specific sulfidation state or coordination of cobalt, but just represents the sites for hydrogen dissociation, while Co_r represents deactivated sites. Eq. (S1) describes the dissociation of molecular hydrogen into sorbed atomic species, HCo, on the Co_9S_8 phase, Eq. (S2) the formation of mobile hydrogen on the Co_9S_8 surface and Eq. (S3) the deactivation of the active sites for hydrogen dissociation on Co_9S_8 by reduction of Co_9S_8. The corresponding equilibrium equations can be written as:

$$K_1 = \frac{[HCo]^2}{[Co]^2 P_{H_2}} \tag{1}$$

$$K_2 = \frac{[Co][H_{so,Co}]}{[HCo]} \tag{2}$$

$$K_3 = \frac{[Co_r]^2 P_{H_2S}}{[Co]^2 [H_{so,Co}]^2} \tag{3}$$

where the concentrations of surface species, i, are represented by $[i]$ with mol/(m^2Co) as unit, the partial pressures (bar) of the gases, H_2 and H_2S, by P_{H_2} and P_{H_2S}, respectively, and the chemical equilibrium constants by K_i. The relative concentration of non-deactivated sites, $1 - \theta_r$, can be defined as:

$$1 - \theta_r = \frac{1 + \sqrt{K_1 P_{H_2}}}{1 + \sqrt{K_1 P_{H_2}} + \sqrt{K_3 P_{H_2S}}\,[H_{so,Co}]}, \tag{3-1}$$

and from Eqs. (1) and (2), the concentration of spillover hydrogen on donor can be calculated by the formula:

$$[H_{so,Co}] = K_2 \sqrt{K_1 P_{H_2}} \tag{3-2}$$

The migration step, which can in principle be a controlling step, may be described as:

$$H_{so,Co} \leftrightarrow H_{so,Mo} \tag{S4}$$

where the symbols $H_{so,Co}$ and $H_{so,Mo}$ represent, respectively, spillover hydrogen on Co_9S_8 and on MoS_2 and are used only when the distinction is necessary. It is practically impossible to represent the rate of H_{so} migration accurately and, in particular, the gradient of H_{so} concentration, between the point where it is produced and the point of contact between the donor particle and an acceptor particle. The same difficulty exists for the diffusion between this contact point and the point where it is consumed. For the sake of simplicity and taking into account experimental data showing the importance of an intermediate contact between donor (Co_9S_8) and acceptor (MoS_2) [39], it is assumed

that the main factor limiting surface diffusion is the transfer of H_{so} across the point of contact between donor and acceptor for unsupported catalysts. For supported catalysts, diffusion on the support surface may constitute the main factor of rate limitation [40]. In summary, it may generally be sufficient to take into account the diffusion rate between the donor, the diffusion source and the acceptor, which occurs either through direct contact between phases, or through the support surface, according to whether the donor and acceptor are pure or supported. The corresponding lumped rate equation (mol/kg cat s) in a general form can therefore be considered for both supported and unsupported catalysts:

$$r_4 = \frac{D_S S_g S_{Co}\, \rho(1-\theta_r)}{L} \beta \rho_{cat}([H_{so,Co}] - [H_{so,Mo}]) \tag{4}$$

where the specific area of surface S_g can be defined as the specific surface area of the support for supported catalysts and that of active phase (MoS_2) for unsupported catalysts, with the unit of m^2/(kg cat), and the other parameters are defined as follows:

D_s	diffusivity of spillover hydrogen, m^2/s
S_{Co}	the surface area of promoter phase (Co_9S_8), source of the surface diffusion, m^2/(mol Co)
ρ	proportion of the donor, $\rho = Co/(Co + Mo)$ molar ratio
ρ_{cat}	density of the catalyst, kg/m^3
β	the metal loading of catalyst, mol(Co + Mo)/kg cat
L	the diffusion distance, m

3.2. Genesis of the active sites

In the present work, the 3-fold CUS sites, which correspond to the special structure of the edge of a MoS_2 slab schematically shown in Fig. 3, namely when one S(B) atom is removed as H_2S to form two 3-fold CUS's, HYD sites, will be symbolized by τ. Their formation from inactive sites (π, 2-fold CUS sites), can be represented by the following chemical reaction (Fig. 3):

$$2\pi + 2H_{so,Mo} \leftrightarrow 2\tau + H_2S \tag{S5}$$

corresponding to the following equilibrium equation:

$$K_5 = \frac{[\tau]^2 P_{H_2S}}{[\pi]^2 [H_{so,Co}]^2} \tag{5}$$

According to the previous discussion, the formation of HDS sites, σ, is considered here for the three possibilities, which will be described in three different kinetics models, 4-fold CUS sites (S6-1 and Fig. 4A), pair-sites (S6-2 and Fig. 4B) and the SH group involved 3-fold CUS sites (S6-3 and Fig. 4C):

$$2\tau + 2H_{so,Mo} \leftrightarrow 2\sigma + H_2S \text{ (model G)} \tag{S6-1}$$

$$2\tau + 2H_{so,Mo} \leftrightarrow \sigma \text{ (model I)} \tag{S6-2}$$

$$2\tau + 2H_2S \leftrightarrow 2\sigma \text{ (model J)} \tag{S6-3}$$

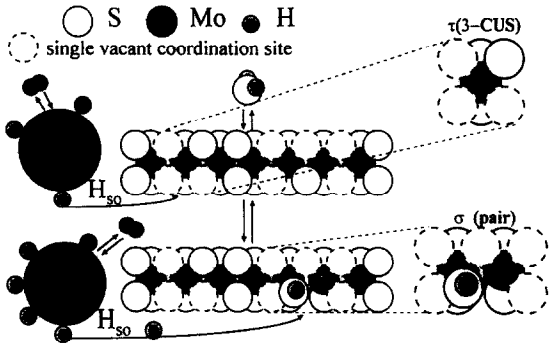

Fig. 5. Remote control and site interconversion (model I).

The corresponding equilibrium relations are represented by the following equations:

$$K_{6\text{-}1} = \frac{[\sigma]^2 P_{H_2S}}{[\tau]^2 [H_{so,Co}]^2} \tag{6-1}$$

$$K_{6\text{-}2} = \frac{[\sigma]}{[\tau]^2 [H_{so,Co}]^2} \tag{6-2}$$

$$K_{6\text{-}3} = \frac{[\sigma]^2}{[\tau]^2 P_{H_2S}} \tag{6-3}$$

In order to assist the readers, we represent schematically the τ and σ sites in Fig. 5. Fig. 5 reflects the generally accepted fact that HYD sites are 3-fold uncoordinated sites (3-CUS Mo). With respect to the σ sites we did not attempt to represent all possible structures, but just the one we tentatively proposed as probable, namely a twin site constituted of one 3-fold uncoordinated Mo carrying an SH group and one 4-fold uncoordinated Mo (with, in the figure, one H occupying one of those unsaturated coordinations). We have to represent here a process in which CoS_x releases mobile hydrogen atoms/protons, which migrate from CoS_x to MoS_2 and react with the (1010) edges of an MoS_2 slab (Fig. 5), leading to the reduced Mo sites corresponding to HYD (τ) and HDS (σ-pair) sites. The enlarged pictures of these active sites (right part of Fig. 5) show clearly the probable structures of sites for HYD and HDS, respectively.

The HYD and HDS mechanisms on the original sites, which originally exist on the MoS_2 phase, called τ^0 for HYD and σ^0 for HDS, are considered to be the same as on the sites created by spillover hydrogen, namely τ for HYD and σ for HDS. Logically, an interconversion between the original HYD and HDS sites, which are defective structures on MoS_2 with very low coordination, must be assumed, in principle. By analogy these sites may also be deactivated as follows [2,7]:

$$2\tau^0 + H_2S \leftrightarrow \sigma^0 + \delta \tag{S7}$$

with the equilibrium equation:

$$K^0 = \frac{[\sigma^0][\delta]}{[\tau^0]^2 P_{H_2S}} \tag{7}$$

where δ represents the deactivated sites. In order to give self-consistency to the model, an additional relation between $[\sigma^0]$ and $[\delta]$ is needed. It is assumed to be a simple linear relation:

$$[\sigma^0] = k_\delta[\delta]. \tag{8}$$

However, it should be underlined that there is no direct evidence yet to support this interconversion of the so-called original active sites. Some other possibilities may have to be taken into account if a more detailed analysis is desired. This would need a very detailed investigation of the HDS and HYD catalysis phenomena on pure MoS_2 catalysts (without promoter).

The interconversion relation between HYD sites (τ) and inactive sites (π) can be described by (Eq. (5)):

$$[\tau] = a_\tau[\pi] \text{ (for all the models)} \tag{9}$$

where a_τ is the interconversion coefficient between π and τ sites and can be derived from Eq. (5):

$$a_\tau = \sqrt{K_5/P_{H_2S}}\,[H_{so,Mo}] \tag{10}$$

The interconversion relations between the HYD sites (τ) and HDS sites (σ) can be obtained from Eqs. (6-1), (6-2) and (6-3), corresponding to three possibilities considered in this study:

For models G and J:

$$[\sigma] = a_\sigma[\tau] \tag{11}$$

where the interconversion coefficient (between τ and σ), a_σ, is defined by Eqs. (11-1) and (11-2) for model G and model J, respectively (Eqs. (6-1) and (6-3)):

$$a_\sigma = \sqrt{K_{6\text{-}1}/P_{H_2S}}\,[H_{so,Mo}] \tag{11-1}$$

$$a_\sigma = \sqrt{K_{6\text{-}3}/P_{H_2S}}\,. \tag{11-2}$$

For model I:

$$[\sigma] = a_\sigma[\tau]^2 \tag{12}$$

where the interconversion coefficient a_σ is defined as follows (Eq. (6-2)):

$$a_\sigma = \sqrt{K_{6\text{-}2}[H_{so,Mo}]^2}\,. \tag{12-1}$$

Similarly, the interconversion between original sites, τ^0 for HYD and σ^0 for HDS, can be written as:

$$[\sigma^0] = a_\sigma^0[\tau^0] \tag{13}$$

where the interconversion (between τ^0 and σ^0) coefficient a_σ^0 is defined by (Eqs. (7) and (8)):

$$a_\sigma^0 = \sqrt{k_\sigma K_{23} P_{H_2S}} \tag{13-1}$$

for all the models. In summary, the interconversions between sites are uniquely defined by coefficients, a_τ, a_σ and a_σ^0, which are the functions of the partial pressures of hydrogen sulfide and hydrogen (the concentration of spillover hydrogen is the function of the partial pressure of hydrogen), for all three models considered.

3.3. Mechanism of the main reactions

The simulated reaction mixture must reflect the main feature of a real HYD and HDS process. It is assumed, in line with many experimental tests, to consist of thiophene (T), solvent (S), hydrogen (H_2), hydrogen sulfide (H_2S), unsaturated hydrocarbons (i.e. butene) (B) and paraffins (i.e. butane) (A).

The reaction scheme for the HDS of thiophene has been discussed by several authors [2,9,10,41]. It is based on the fact that hydrocarbon products that were experimentally detected were only butane and butenes during thiophene HDS [2,42]:

$$\text{Thiophene} + 3H_2 \xrightarrow[-H_2S]{\text{HDS sites}} \text{Butenes} \xrightarrow[+H_2]{\text{HYD sites}} \text{Butane}$$

and the HYD of unsaturated hydrocarbons (including butenes from HDS) as

$$\text{Unsaturated hydrocarbons} + \text{Butenes} \xrightarrow[+H_2]{\text{HYD sites}} \text{Paraffins} + \text{Butane}$$

The mechanisms of HYD of unsaturated hydrocarbons and HDS of thiophene are not fully understood yet. The mechanism suggested by Van Parijs and Froment [9,10] involved reactions between a sorbed unsaturated molecule on one site (τ/σ) and a sorbed H_2 molecule on another site (τ/σ), reflecting the fact that occupying more sites by sorbed hydrogen seems unnecessary. In this work, whose objective is different from that of these authors, it is sufficient to assume a simple mechanism. This gives more generality to our model. To avoid objections which could be raised by assuming a too precise model, we suppose that the hydrogen atoms needed in HYD and HDS reactions are not necessarily on sites different from those occupied by unsaturated hydrocarbons or thiophene, but possibly on the metal sites where unsaturated hydrocarbons or thiophene are sorbed or on the sulfur sites in the vicinity of the sorbed unsaturated hydrocarbons or thiophene. This assumption corresponds to the fact that sorbed hydrogen atoms are likely to be present in large quantities on the surface in an environment where molecular hydrogen is dominant (especially at high pressures) and are very mobile. This does not come into conflict with the implications of the results of Van Parijs and Froment [9,10]. A comprehensive HDS mechanism was suggested by Delmon and Dallons, in which a group of two cooperating sites was proposed [36]. This assumption is close to (but not the same as) the sites represented in Fig. 4B or C. The mechanism used here also considers the fact that butenes and butane are the only detected products in thiophene HDS [2,9,10,36]. The mechanisms of HDS of thiophene and HYD of unsaturated hydrocarbons (including butene from HDS) are summarized in Table 1.

In Table 1, the first three steps (S7–S9) describe the HYD reaction on τ sites. Step S7 represents the dissociative adsorption of molecular hydrogen on a τ site (the modification of a τ site by atomic hydrogen), step S8 represents the adsorption of unsaturated hydrocarbons on the modified τ sites and the rate controlling step (S9) represents the hydrogenation of sorbed unsaturated hydrocarbons into paraffin products which get immediately desorbed from the τ sites.

The following 5 steps (S10 to S14) describe the HDS of thiophene. The σ sites are initially modified by dissociative adsorption of molecular hydrogen (step S10). Thiophene molecules are adsorbed and partially hydrogenated on the modified σ sites (step S11), the σ sites with the partially hydrogenated thiophene species dissociatively adsorb a hydrogen molecule (step 12) and then a rate

Table 1
HDS and HYD mechanism (following Eqs. (S6-1), (S6-2) and (S6-3) in the text) [a]

Step Si HYD/HDS mechanism	Equilibrium or rate equations	Concentrations of surface species/Notes
(7) $\tau + H_2 \leftrightarrow H\cdot\tau\cdot H$	$K_7 = [H\cdot\tau\cdot H]/[\tau]P_{H_2}$	$[H\cdot\tau\cdot H] = K_7 P_{H_2}[\tau]$
(8) $H\cdot\tau\cdot H + B \leftrightarrow {}^{B}_{H\cdot\tau\cdot H}$	$K_8 = \left[{}^{B}_{H\cdot\tau\cdot H}\right]/[H\cdot\tau\cdot H]P_B$	$\left[{}^{B}_{H\cdot\tau\cdot H}\right] = K_7K_8P_{H_2}PB[\tau]$
(9) ${}^{B}_{H\cdot\tau\cdot H} \rightarrow \tau + A$	$r_9 = k_{90}\left[{}^{B}_{H\cdot\tau\cdot H}\right]$	
(10) $\sigma + H_2 \leftrightarrow H\cdot\sigma\cdot H$	$K_{10} = [H\cdot\sigma\cdot H]/[\sigma]P_{H_2}$	$[H\cdot\sigma\cdot H] = K_{10}P_{H_2}[\sigma]$
(11) $H\cdot\sigma\cdot H + T \leftrightarrow \sigma\cdot T^{=}$	$K_{11} = [\sigma\cdot T^{=}]/[H\cdot\sigma\cdot H]P_T$	$[\sigma\cdot T^{=}] = K_{10}K_{11}P_{H_2}P_T[\sigma]$
(12) $\sigma\cdot T^{=} + H_2 \leftrightarrow {}^{T^{=}}_{H\cdot\tau\cdot H}$	$K_{12} = \left[{}^{T^{=}}_{H\cdot\tau\cdot H}\right]/[\sigma\cdot T^{=}]P_{H_2}$	$\left[{}^{T^{=}}_{H\cdot\tau\cdot H}\right] = K_{10}K_{11}K_{12}P_{H_2}^2P_T[\sigma]$
(13) ${}^{T^{=}}_{H\cdot\tau\cdot H} \rightarrow \sigma\cdot S + B$	$r_{13} = k_{130}\left[{}^{T^{=}}_{H\cdot\tau\cdot H}\right]$	$r_c \ll r_{13}$, loss of H_{so} is negligible compared to H_2 consumption in main reaction
(13-1) $\sigma\cdot S + 2H_{so,Mo} \rightarrow \sigma + H_2S$	$r_c = k_c[\sigma\cdot S][H_{so,Mo}]^2$	
(14) $\sigma\cdot S + H_2 \leftrightarrow \sigma + H_2S$	$K_{14} = [\sigma]P_{H_2S}/[\sigma\cdot S]P_{H_2}$	$[\sigma\cdot S] = P_{H_2S}(K_{14}P_{H_2})^{-1}[\sigma]$
(15) $\tau^0 + H_2 \leftrightarrow H\cdot\tau^0\cdot H$	$K_7 = [H\cdot\tau^0\cdot H]/[\tau^0]P_{H_2}$	$[H\cdot\tau^0\cdot H] = K_7P_{H_2}[\tau^0]$
(16) $H\cdot\tau^0\cdot H + B \leftrightarrow {}^{B}_{H\cdot\tau^0\cdot H}$	$K_8 = \left[{}^{B}_{H\cdot\tau^0\cdot H}\right]/[H\cdot\tau^0\cdot H]P_B$	$\left[{}^{B}_{H\cdot\tau^0\cdot H}\right] = K_7K_8P_{H_2}P_B[\tau^0]$
(17) ${}^{B}_{H\cdot\tau^0\cdot H} \rightarrow \tau^0 + A$	$r_{17} = k_{90}\left[{}^{B}_{H\cdot\tau^0\cdot H}\right]$	
(18) $\sigma^0 + H_2 \leftrightarrow H\cdot\sigma^0\cdot H$	$K_{10} = [H\cdot\sigma^0\cdot H]/[\sigma^0]P_{H_2}$	$[H\cdot\sigma^0\cdot H] = K_{10}P_{H_2}[\sigma^0]$
(19) $H\cdot\sigma^0\cdot H + T \leftrightarrow \sigma^0\cdot T^{=}$	$K_{11} = [\sigma^0\cdot T^{=}]/[H\cdot\sigma^0\cdot H]P_T$	$[\sigma^0\cdot T^{=}] = K_{10}K_{11}P_{H_2}P_T[\sigma^0]$
(20) $\sigma\cdot T^{=} + H_2 \leftrightarrow {}^{T^{=}}_{H\cdot\sigma^0\cdot H}$	$K_{12} = \left[{}^{T^{=}}_{H\cdot\sigma^0\cdot H}\right]/[\sigma^0\cdot T^{=}]P_{H_2}$	$\left[{}^{T^{=}}_{H\cdot\sigma^0\cdot H}\right] = K_{10}K_{11}K_{12}P_{H_2}^2P_T[\sigma^0]$
(21) ${}^{T^{=}}_{H\cdot\sigma^0\cdot H} \rightarrow \sigma^0\cdot S + B$	$r_{21} = k_{130}\left[{}^{T^{=}}_{H\cdot\sigma^0\cdot H}\right]$	
(22) $\sigma^0\cdot S + H_2 \leftrightarrow \sigma^0 + H_2S$	$K_{14} = [\sigma^0]P_{H_2S}/[\sigma^0\cdot S]P_{H_2}$	$[\sigma^0\cdot S] = P_{H_2S}(K_{14}P_{H_2})^{-1}[\sigma^0]$

controlling step (S13) follows: the resulting sulfur containing species are hydrogenolysed, producing butene molecules and sulfur occupied σ sites. Finally, the S atoms left on σ sites from step S13 are hydrogenated in an equilibrium step (S14). The mechanisms on the original sites (τ^0 and σ^0) are assumed to be the same as those on sites created by spillover hydrogen (τ and σ), which are simply repeated in steps S15 to S22. In addition, it should be noted that a step for describing the consumption of spillover hydrogen on the MoS_2 surface is assumed in step S13-1, which represents the reaction between two mobile H_{so} species with one deposited S atom on σ sites coming from step S13. For all these elementary steps, the corresponding mathematical expressions (equilibrium equations or rate equations) are also listed in Table 1 (two columns at the right).

3.4. Dynamics of spillover H_{so}

The consumption of $H_{so,Mo}$ on the acceptor takes into account the fact that spillover hydrogen may react with the sulfur (step S13-1 in Table 1) depositing on HDS sites because of the HDS of thiophene. The rate of this step (S13-1) can be rewritten as (Table 1):

$$r_c = k_c P_{H_2S}\left(K_{14}P_{H_2}\right)^{-1}\left[H_{so,Mo}\right]^2[\sigma] \tag{14}$$

[a] $T^{=}$ represents the partially hydrogenated thiophene,

with the unit of mol/m^2 Mo s. The net rate of the H_{so} accumulation on the acceptor can be obtained by subtracting the rate of consumption in Eq. (14) from the rate of diffusion in Eq. (4):

$$r_{H_{so}} = r_4/[\beta(1-\rho)S_{Mo}] - r_c. \tag{15}$$

The dynamic changing of the surface concentration of spillover H_{so} on the acceptor can then be uniquely defined as:

$$\frac{d[H_{so,Mo}]}{dt} = r^2_{H_{so}} \tag{16}$$

3.5. Final kinetic equations

By combining the spillover mechanism, the remote control, developed in Sections 3.1 and 3.2 with those for main reactions in Section 3.3, the conservation of metal sites for the created sites and the original sites, respectively, can be applied as follows:

$$\Sigma[{}^*\tau] + \Sigma[{}^*\sigma] + [\pi] = [Mo]_t \tag{17}$$

$$\Sigma[{}^*\tau^0] + \Sigma[{}^*\sigma^0] + [\delta] = [Mo]^0_t \tag{18}$$

where '*' indicates the species related to the kind of sites considered, namely HYD, HDS and empty sites, and $[Mo]_t$ and $[Mo]^0_t$ represent the total concentrations of metal sites on edges, those which are activated by spillover hydrogen and those originally active because of the defective structure of the MoS_2 slabs. The total concentration of τ related species can be obtained by the sum of the concentrations of available τ sites and the species sorbed on τ sites:

$$\Sigma[\tau^*] = [\tau] + [H\cdot\tau\cdot H] + \begin{bmatrix} B \\ H\cdot\tau\cdot H \end{bmatrix} \tag{19}$$

Substituting the related formula listed in Table 1 into Eq. (19) and taking into account the interconversion relationship (Eqs. (9) and (10)) leads to:

$$\Sigma[\tau^*] = a_\tau(1 + K_7P_{H_2} + K_7K_8P_{H_2}P_B)[\pi] \tag{19-1}$$

Similarly, the total concentration of σ related species can be obtained by the sum of the concentrations of available σ sites and the species sorbed on σ sites:

$$\Sigma[\sigma^*] = [\sigma] + [H\cdot\sigma\cdot H] + [\sigma\cdot T^=]\begin{bmatrix} T^= \\ H\cdot\sigma\cdot H \end{bmatrix} + [\sigma\cdot S] \tag{20}$$

By substituting the related formula listed in Table 1 and the interconversion relations (Eqs. (11) and (12) into Eq. (20), the sum can be written as:

$$\Sigma[\sigma^*] = a_\tau a_\sigma\left[1 + K_{10}P_{H_2} + K_{10}K_{11}P_TP_{H_2} + K_{10}K_{11}K_{12}P_TP^2_{H_2} + P_{H_2S}(K_{14}P_{H_2})^{-1}\right][\pi] \tag{20-1}$$

for model G and model J and

$$\Sigma[\sigma^*] = 2a_\tau a^2_\sigma\left[1 + K_{10}P_{H_2} + K_{10}K_{11}P_TP_{H_2} + K_{10}K_{11}K_{12}P_TP^2_{H_2} + P_{H_2S}(K_{14}P_{H_2})^{-1}\right][\pi]^2 \tag{20-2}$$

for model I. In Eq. (20-2), the fact that two metal sites are involved in each HDS site is reflected by the factor 2 and the term $[\pi]^2$.

By substituting Eqs. (19-1) and (20-1) into Eq. (17) and rearranging the result equation, the surface concentrations of π can be obtained:

$$[\pi] = [\mathrm{Mo}]_t / \left\{1 + a_\tau\left(1 + K_7 P_{H_2} + K_7 K_8 P_{H_2} P_B\right) + a_\tau a_\sigma \left[1 + K_{10} P_{H_2} + K_{10} K_{11} P_T P_{H_2} + K_{10} K_{11} K_{12} P_T P_{H_2}^2 + P_{H_2S}\left(K_{14} P_{H_2}\right)^{-1}\right]\right\} \quad (21)$$

for model G and model J and

$$[\pi] = \frac{2[\mathrm{Mo}]t}{A_2 + \sqrt{A_2^2 + 4A_1[\mathrm{Mo}]_t}} \quad (22)$$

for model I, where

$$A_1 = 2a_\tau^2 a_\sigma \left[1 + K_{10} P_{H_2} + K_{10} K_{11} P_T P_{H_2} + K_{10} K_{11} K_{12} P_T P_{H_2}^2 + P_{H_2S}\left(K_{14} P_{H_2}\right)^{-1}\right] \quad (22\text{-}1)$$

$$A_2 = \left[1 + a_\tau\left(1 + K_7 P_{H_2} + K_7 K_8 P_{H_2} P_B\right)\right]. \quad (22\text{-}2)$$

Similar treatment for the metal site conservation (Eq. (18)) of original sites can be applied and a general formula for all models can be obtained:

$$[\tau^0] = [\mathrm{Mo}]_t^0 / \left\{1 + K_7 P_{H_2} + K_7 K_8 P_{H_2} P_B) + a_\sigma^0 \left[1 + k_\sigma^{-1} + K_{10} P_{H_2} + K_{10} K_{11} P_T P_{H_2} + K_{10} K_{11} K_{12} P_T P_{H_2}^2 + P_{H_2S}\left(K_{14} P_{H_2}\right)^{-1}\right]\right\} \quad (23)$$

By rewriting the rate expressions listed in Table 1 and substituting the terms related to surface concentrations of various species in these equations, the following rate equations (rate unit: mol/m^2 Mo s) giving rates on the various sites can be obtained: for HYD on τ sites (step S9 in Table 1)

$$r_9 = k_{90} K_7 K_8 P_{H_2} P_B a_\tau [\pi] \text{ (all models)} \quad (24)$$

and on τ^0 sites (step S17 in Table 1)

$$r_{17} = k_{90} K_7 K_8 P_{H_2} P_B [\tau^0], \quad (25)$$

and for HDS on σ sites (step S13)

$$r_{13} = k_{130} K_{10} K_{11} K_{12} P_{H_2}^2 P_T a_\tau a_\sigma [\pi] \text{ (model G and J)} \quad (26)$$

$$r_{13} = k_{130} K_{10} K_{11} K_{12} P_{H_2}^2 P_T a_\tau^2 a_\sigma [\pi]^2 \text{ (model I)} \quad (27)$$

and on σ^0 sites (step S21)

$$r_{21} = k_{130} K_{10} K_{11} K_{12} P_{H_2}^2 P_T a_\sigma^0 [\tau^0] \quad (28)$$

The total HYD rate is the sum of the rates of step S9 and step S17 (Table 1):

$$r_{HYD} = (r_9 + r_{17})\beta(1-\rho)S_{Mo}, \tag{29}$$

and total HDS rate:

$$r_{HDS} = (r_{13} + r_{21})\beta(1-\rho)S_{Mo}. \tag{29-1}$$

The unit of these rates in Eqs. (29) and (29-1) is (mol/kg cat s). These kinetic equations can be combined into a reactor model to simulate various cases corresponding to hydrotreating experiments. This will be discussed in Section 4.

4. Organization of the simulation program

4.1. Reactor model

The CST reactor is selected to investigate the present kinetic models simply because it is possible to simulate both the dynamic and steady state trends of hydrotreating catalysis by combining the present kinetics models. Any other type of reactors would introduce a complexity, especially in numerical treatment, which is unnecessary in this work.

A CST reactor is represented schematically in Fig. 6. If the volume of the catalyst bed is V_R (m^3) and its void space ε_B, the material balances through the reactor, using the operation parameters indicated in Fig. 6, correspond to the following differential equations:

$$\frac{dx_T}{dt} = \frac{1}{\varepsilon_B V_R}\left(F^0 x_T^0 - F x_T\right) + \frac{R_g T}{P}\cdot\frac{\rho_{cat}(1-\varepsilon_B)}{\varepsilon_B}(-r_{HDS}) \tag{30}$$

$$\frac{dX_B}{dt} = \frac{1}{\varepsilon_B V_R}\left(F^0 x_B^0 - F x_B\right) + \frac{R_g T}{P}\cdot\frac{\rho_{cat}(1-\varepsilon_B)}{\varepsilon_B}(r_{HDS} - r_{HYD}) \tag{31}$$

$$\frac{dx_A}{dt} = \frac{1}{\varepsilon_B V_R}\left(F^0 x_A^0 - F x_A\right) + \frac{R_g T}{P}\cdot\frac{\rho_{cat}(1-\varepsilon_B)}{\varepsilon_B}(r_{HYD}) \tag{32}$$

$$\frac{dx_{H_2}}{dt} = \frac{1}{\varepsilon_B V_R}\left(F^0 x_{H_2}^0 - F x_{H_2}\right) + \frac{R_g T}{P}\cdot\frac{\rho_{cat}(1-\varepsilon_B)}{\varepsilon_B}(-3r_{HDS} - r_{HYD}) \tag{33}$$

$$\frac{dx_{H_2S}}{dt} = \frac{1}{\varepsilon_B V_R}\left(F^0 x_{H_2S}^0 - F x_{H_2S}\right) + \frac{R_g T}{P}\cdot\frac{\rho_{cat}(1-\varepsilon_B)}{\varepsilon_B} r_{HDS} \tag{34}$$

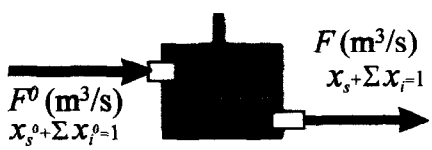

x = mole fraction

s = solvent; i = thiophene, H_2, H_2S, -C=C-, butane.

Fig. 6. A CST reactor.

These equations describe the material balances for thiophene (T), unsaturated hydrocarbons (B), paraffins (A), hydrogen and hydrogen sulfide. In these equations, T is temperature in K, P is total pressure in bar, R_g is the gas constant (8.314 J/mol K), ρ_{cat} is apparent density of catalyst particles in kg/m^3 and x_i^0 and x_i represent the mole fractions of component i in the feed and in the reactor bulk, respectively. In Eqs. (30)–(34), the rates of the changes of the mole fractions in the reactor (left sides of equations) consist of the hydrodynamic replacement represented by the first term of right sides and the chemical reaction (kinetics) effect represented by the second term.

Care must be taken that the dynamics of spillover H_{so} represented by Eq. (16) have to be combined into the dynamic equations (Eqs. (30)–(34) defined by the material balances over a CST reactor. Eq. (16) provides the necessary information about the dynamics of the surface concentration of spillover hydrogen, which has to be calculated to determine the coefficients of site interconversion, a_τ, a_σ and a_σ^0 in the kinetic models.

In agreement with most experimental data available, the activities used in this article are defined by conversion, if no other specification is made, and calculated as follows:

$$X_{HDS} = \frac{x_T^0 F^0 - x_T F}{x_T^0 F^0} \tag{35}$$

$$X_{HYD} = \frac{F^0 x_B^0 - x_B F}{F^0 x_{BT}^0 + x_T^0 F^0 - x_T F} \tag{36}$$

where the mole fractions of thiophene and unsaturated hydrocarbons, x_T and x_B and the flow rate at the outlet of the reactor, F, are calculated by integrating Eqs. (30)–(34) together with Eq. (16).

4.2. Simulation program

A program to solve this model is coded in Fortran language, in which Eqs. (16), (30)–(34) are integrated by using a fifth–sixth order Runge–Kutta routine from Netlib on Internet free sites. The program uses an approach similar to that of Rebitzki et al. [13] to simulate both the dynamic behaviors and the steady states of a CST reactor. The criterion for the convergence of the integration to a steady state is that the relative deviations of the conversions of thiophene and unsaturated hydrocarbons between two sequential time points are both less than 10^{-5}. The integration tolerance is set to 10^{-8}. The flow sheet of the program is shown in Fig. 7. The program reads data from an input file to initialize a simulation task. The input data file contains all the necessary data defining the properties of catalysts and the reactor, and the information controlling the program to perform a desired simulation. According to the input indication, one of the three tasks can be executed. After a task is finished, all the results from the simulation are stored in an output file with a name defined in the input file by users, which can be analyzed by any proper standard software like MS-EXCEL. The three functional modules are:

Synergy simulator: This module is designed to simulate the variations of the system at steady states as a function of the proportion of donor in catalysts. The flow sheet is shown in Fig. 7. In Fig. 7, $\boldsymbol{x}$ and $\boldsymbol{x}_0$ represent, respectively, the vector of mole fractions at the outlet of the reactor and the initial guess of the vector and $\boldsymbol{X}$ and $\boldsymbol{X}_0$ represent the vector of conversions, namely (X_{HDS}, X_{HYD}) and its previous value, respectively. Eqs. (16), (30)–(34) (kinetic models in Fig. 7) are integrated to a steady

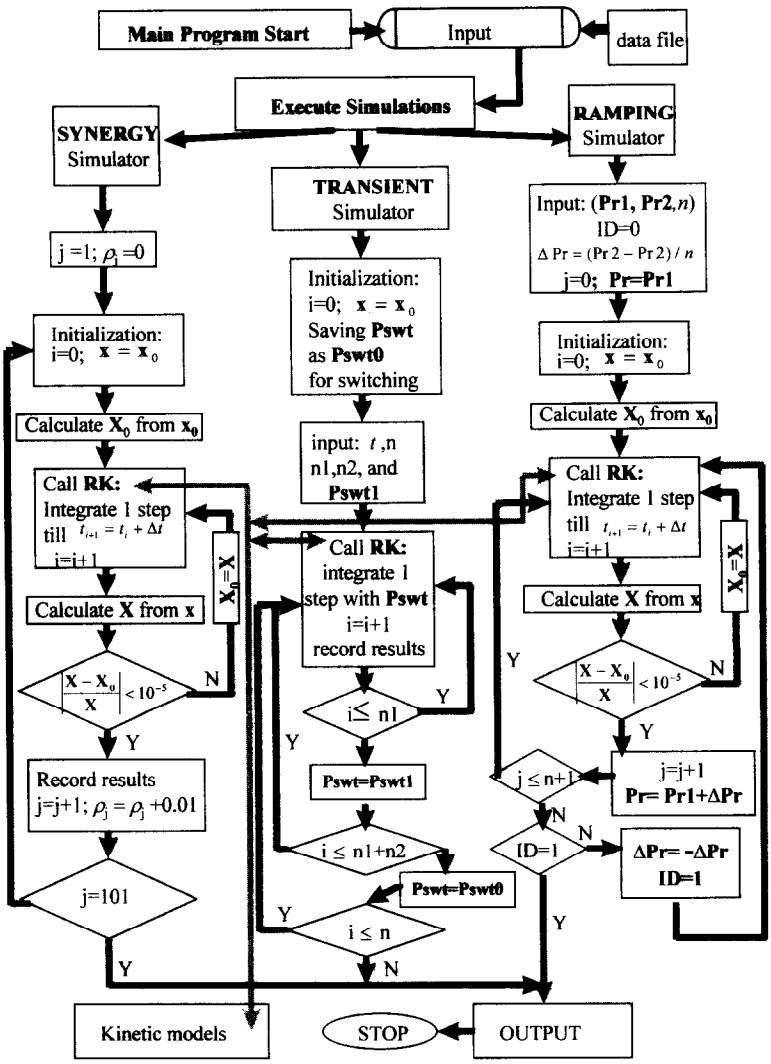

Fig. 7. Simulator of the HYD and HDS kinetics.

state by calling the integration subroutine **RK** for 100 values of the proportion of donor, ρ, which are uniformly increased from 0 to 1. The results at the final steady state for each ρ value are recorded. Synergy behaviors can be simulated by calling this module.

Transient simulator: This module is designed to calculate and record the transient trajectories of the system variables (the second column in Fig. 7). The time (t) for which the integration has to be done and the number of integration steps (n) is input into the simulator. In order to simulate a switching operation, an intermediate value of a defined switching parameter, **Pswt** in Fig. 7, which can be x_T, x_{H_2S}, x_B or P, along with the step numbers, $n1$ and $n2$, for, respectively, the first and the second switching stages, is asked by the simulator. From a given initial state of the reactor, the simulator integrates, by calling **RK**, Eqs. (16), (30)–(34) (kinetic models in Fig. 7) to $n1(\Delta t)$ with a given step size ($\Delta t = t/n$), then sets **Pswt** = **Pswt1** (switch to new value) and integrates again Eqs. (16), (30)–(34) to $(n1 + n2)(\Delta t)$ with the step size, Δt, and finally sets **Pswt** = **Pswt0** (switch back) and

Table 2
Parameters for all models

Parameters	Values	Parameters	Values
K_1 (bar^{-1})	0.47	K_{12} (bar^{-1})	0.5
K_3 (bar $(mol/m^2\ Co)^{-2}$)	1.95E5	K_{14}	40.0
$D_{S,0}$ (m^2/s)	1.8E−10	k_c ($(mol/m^2\ Mo)^{-2}\ s^{-1}$)	1E18
E_S (J/mol)	117152.0	$[Mo]_t^0/[Mo]_t$	0.1
L (m)	2E−9	$[Mo]_t$ (mol/m^2 Mo)	5E−7
K_7, K^0 (bar^{-1})	8.2E−3	β (mol/kg cat)	1.9
K_8 (bar^{-1})	3.98	S_{Co} (m^2/mol)	10000
K_{10} (bar^{-1})	0.16	S_{Mo} (m^2/mol)	10000
K_{11} (bar^{-1})	4.32	ρ_{cat} (kg/m^3)	1200

integrates until t. All the values of variables are recorded at each integration step. For non-switching simulation, the instruction **Pswt1 = Pswt0** is set.

Ramping simulator: This module integrates Eqs. (16), (30)–(34) to steady states and records the steady state results at each value of a ramping parameter, **Pr**, which is changed uniformly by an upper loop from an initial value **Pr1** to an end value **Pr2** with a given step size ($\Delta Pr = (Pr2 - Pr1)/n$) (Fig. 7). As soon as the value of the ramping parameter **Pr** is equal to the end value **Pr2**, the program sets a new initial value equal to **Pr2** and a new end value to **Pr1** and repeats the above integration, with $\Delta Pr = -(Pr2 - Pr1)/n$, until **Pr = Pr1**. The initial values of variables for Eqs. (16), (30)–(34) at a certain ramping point are set to the steady state values of these variables at last ramping point (Fig. 7).

4.3. Estimation of parameters

4.3.1. Kinetic parameters

The parameters for the kinetic models discussed above are mainly determined on the basis of those reported in literature [2,12,38,42,43]. The system is less sensitive to certain parameters, for example some of the equilibrium constants. These parameters are generally taken within a range of several magnitudes. The value of the diffusivity of spillover hydrogen is determined according to the reported data for hydrogen spillover on alumina [40]. The rate constants of the non-equilibrium steps, to which the system is kinetically more sensitive in our cases, are numerically manipulated so as to get an optimal representative of the synergetic trends observed in experiments (in shape and magnitude). These parameters assumed to be the same for all models are listed in Table 2. The other parameters, which are different for the different kinetic models, are listed in Table 3.

Table 3
Parameters for different models

Parameters	Model G	Model I[1]	Model J
Step 6-x	6-1	6-2	6-3
K_2 (mol/m^2 Co)	4.5618E−8	3.9532E−8	5.9360E−8
K_5 (bar $(mol/m^2\ Co)^{-2}$)	2E11	1E12	6.5E10
$K_{6\text{-}1}$, $K_{6\text{-}2}$ and $K_{6\text{-}3}$	2E12 (bar $(mol/m^2\ Co)^{-2}$)	2E22 ($(mol/m^2\ Co)^{-3}$)	0.02 (bar^{-1})
k_{90} (s^{-1})	50	40	50.0
k_{130} (s^{-1})	0.8	0.8	0.8
k_δ	1.2593	0.5	0.54681

Table 4
Feeds and operation conditions

Components	Low H_2S conc. (mole fraction)	High H_2S conc. (mole fraction)
Thiophene (T)	0.0024	0.0024
Solvent (S)	0.12	0.12
Hydrogen (H_2)	0.8386	0.8526
Hydrogen sulfide (H_2S)	0.001	0.015
Butene (B)	0.024	0.024
Butane (A)	0.0	0.0
Space time (kg cat h/kmol liquid)	5	
Pressure, P (bar)	1–100	
Temperature, T (K)	350°C	

4.3.2. Reactor parameters and operation conditions

The basis of the simulation is, for convenience, a reactor loading 1 kg catalyst and the void space of the catalyst bed is $\varepsilon_B = 0.4$, which is assumed as the same as the normal value of a fixed bed. The effective volume of the reactor can be deduced:

$$V_R = 1/[\rho_{cat}(1 - \varepsilon_B)] \tag{37}$$

The feed compositions and flow rate are selected within the range normally used in experiments [2,9,10]. All the data related to reactor operation are summarized in Table 4. The change of the operation conditions will be indicated separately.

5. Simulation and discussion

The models investigated are summarized in Table 5, in which only models G, I and J are discussed in detail. Models A to F were developed simply by combining the remote control theory with the HYD and HDS mechanisms similar to those proposed by Van Parijs and Froment [9,10] and used the following formula to express site interconversion:

$$n\pi + 2H_{so,Mo} \leftrightarrow n\tau + H_2S \tag{S5PP}$$

$$m\tau + 2H_{so,Mo} \leftrightarrow m\sigma + H_2S \tag{S6PP}$$

Table 5
Models investigated in this work [a]

Models	Site interconversion	HYD/HDS mechanism
A	$(m, n, a) = (4, 2, 2)$	Van Parijs and Froment [9,10]
B	$(m, n, a) = (4, 4, 2)$	Van Parijs and Froment [9,10]
C	$(m, n, a) = (2, 2, 2)$	Van Parijs and Froment [9,10]
D	$(m, n, a) = (3, 2, 2)$	Van Parijs and Froment [9,10]
E	$(m, n, a) = (3, 4, 2)$	Van Parijs and Froment [9,10]
F	$(m, n, a) = (4, 2, 2)$	Van Parijs and Froment [9,10]
G	discussed in text	Table 1
H	$(m, n) = (2, 2)$ no H_2S in (S6)	Table 1
I	discussed in text	Table 1
J	discussed in text	Table 1

[a] a is a parameter related to the hydrogen adsorption on HYD sites: $a = 1$, molecular adsorption; $a = 2$, dissociated adsorption.

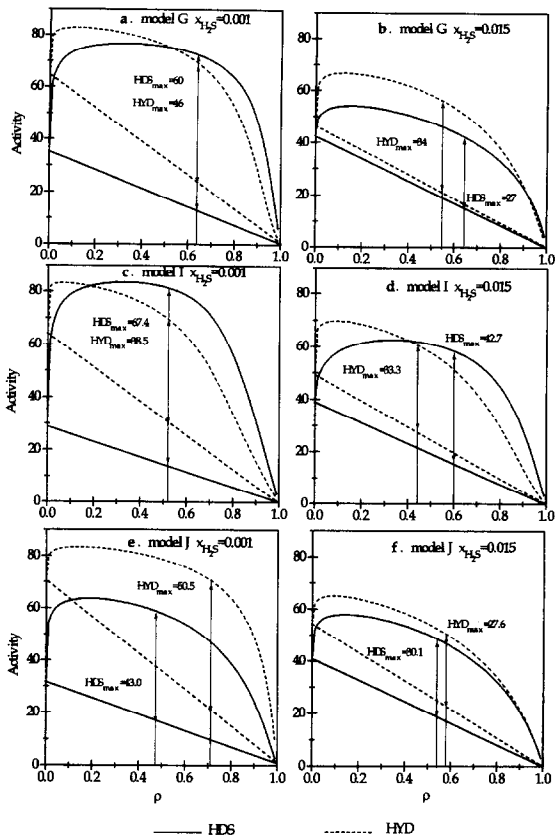

Fig. 8. Simulated synergy curves: operation conditions are listed in Table 4.

where the arbitrary parameters m and n are listed in Table 5. The parameter a in Table 5 represents the number of sites for the adsorption of one H_2 ($a = 1$, molecular adsorption; $a = 2$, dissociated adsorption, see Refs. [9,10]). These six models (A to F) could correctly produce synergy curves. However, they were finally eliminated from this article because they did not take precisely into account the structures of catalytic surfaces and active sites, namely the steps (S5PP and S6PP) do not correspond to the specific surface structure of MoS_2 catalysts. Model H was close to model G, but used arbitrary assumptions about active sites, namely the site interconversion step (S6 for H) could not correctly reflect the structure of HDS sites and was hence excluded. Remaining models (G, I and J) represent three possibilities of precisely defined active sites for HDS as discussed in previous sections, which allow us to avoid complication in the discrimination of models.

The main features of the models described above are expected, at first, to give a correct description of the synergetic effects observed in the HDS and HYD catalysis. All the models considered in this work satisfactorily simulate the synergetic curves, namely the variations of activities with the composition of catalyst, $\rho = Co/(Co + Mo)$, under typical hydrotreating conditions, namely $T =$ 350°C and $P = 60$ bar. Two kinds of feeds are considered (Table 4). The results are summarized in Fig. 8. The simulation with all three models shows that the H_2S concentration in the feed can significantly influence the synergy effect. Higher H_2S concentrations lead to weaker synergy effects for both HYD and HDS. The maximum synergy effects and their positions are also indicated in Fig. 8. For model G, the synergy effect on HDS is larger than on HYD at the low H_2S (Fig. 8a), but a

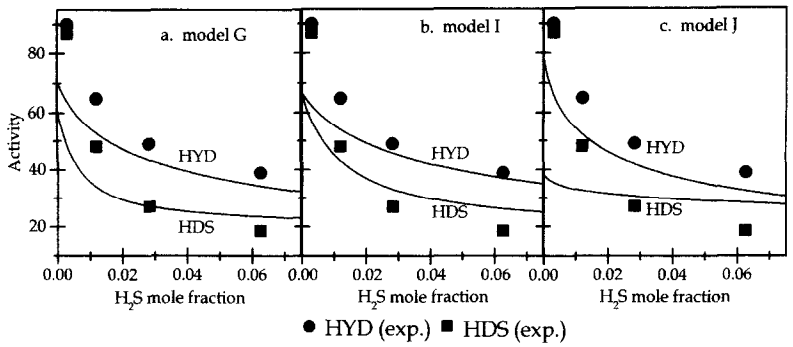

Fig. 9. Influence of the H_2S on HYD and HDS activities. $P = 40$ bar, $p = 0.3$ (experimental points see Ref. [41]).

reversed order is observed at high H_2S concentrations (Fig. 8b). For model I, however, the synergy effect on HDS is always larger than on HYD (Fig. 8c and d). For model J, the synergy effects vary oppositely to model G. As a whole, it may be concluded that the remote control with interconversion between HYD and HDS sites can lead to models that satisfactorily reflect the synergetic behaviors observed in real HDS and HYD catalysis. However, the discrimination between models seems difficult by using only the simulated synergy results.

The influence of H_2S on both HDS and HYD activities has been observed experimentally for a long time [7,8,44–46]. The kinetic models developed here represent the H_2S effect on both HDS and HYD activities. The simulation results concerning the variations of the HDS and HYD activities with the H_2S concentration in the feed of the CST reactor are shown in Fig. 9 (curves). The conditions assumed in this simulation are those used in literature [44] in order to permit a comparison with experimental data. These are $P = 40$ bar with the following mole fractions in the feed: $x_T = 0.00365$, $x_S = 0.01714$, $x_B = 0.0015$ and $x_{H_2+H_2S} = 0.9778$. All three models predict that H_2S inhibits both HDS and HYD activities. The theoretical curves reflect qualitatively the experimental observations, as shown in Fig. 9 (circles: HYD, squares: HDS) [44]. Models G and I both show that the HDS activity is more depressed than the HYD activity by the increase of the H_2S partial pressure in the feed (Fig. 9a and b). The trend predicted by model J, however, is opposite (Fig. 9c), namely the HYD activity is much more depressed than the HDS activity by the increase of the H_2S pressure. Model J cannot reflect the real situation, namely the site interconversion mechanism. Although it is difficult to conclude categorically that the site interconversion is not due to the H_2S as assumed by model J, our results suggest that the predominant role in the interconversion between HYD sites and HDS sites is that of spillover hydrogen as assumed by models G and I. The detailed mechanism of this interconversion along with the exact structure of HYD and HDS sites should be discriminated by more elaborate experimental data using kinetic measurements specially designed for that purpose.

Models G and I have a similar behavior. The following modelling only uses model I to avoid lengthy discussion.

We simulated transient phenomena in several cases. The first case is the transient behavior during the start up of the HYD and HDS catalytic reactions. In real experiments, such phenomena occur after the sulfidation (pretreatment) of catalysts. Experimental transient behaviors of this kind were reported nearly twenty years ago [47], as shown in Fig. 10(a and c) in which the relative activity C_t/C_1 was defined by the ratio of the conversion at t (h) to that at $t = 1$ (h). The authors explained correctly that the difference between transient behaviors of the HDS and HYD activities in a given catalyst was due to the existence of different sites needed for HYD and HDS, respectively. However, no detailed

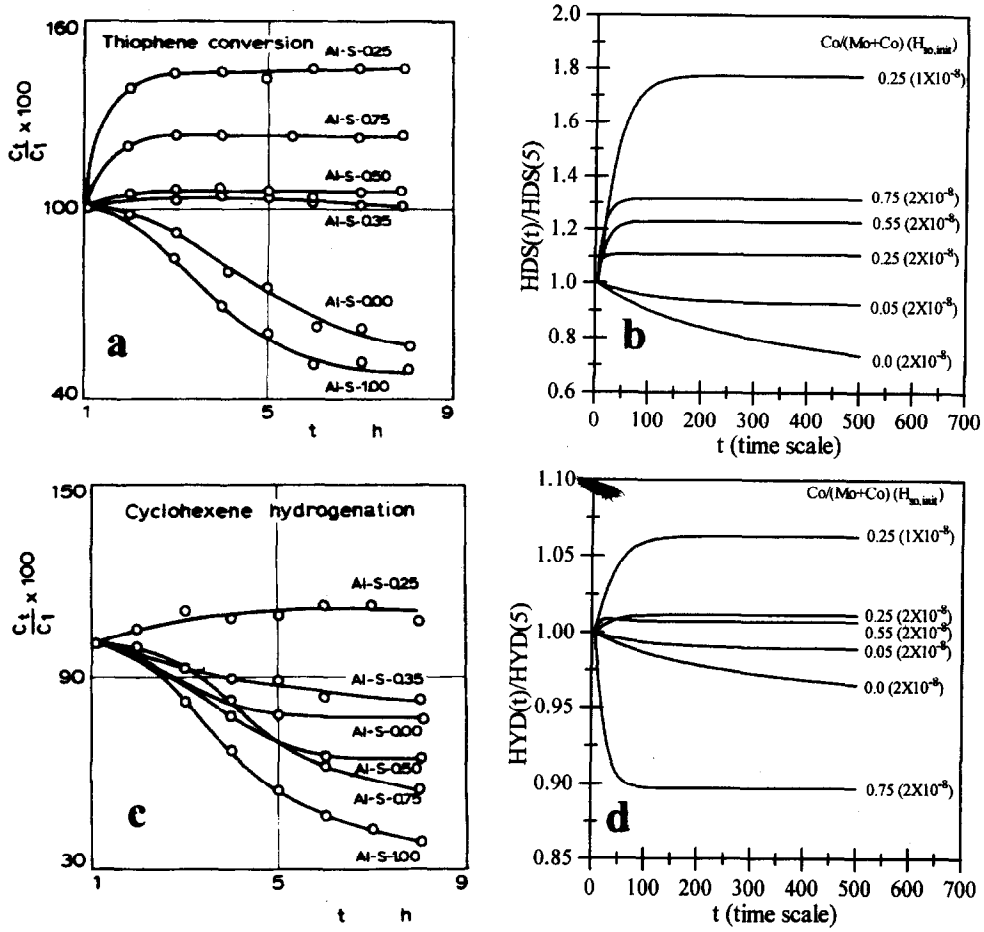

Fig. 10. Comparison of experimental transient trends with those from simulation (model b: the simulation conditions are listed in Table 4 (the group of higher H_2S concentration, $P = 60$ bar).

explanation about the mechanism was provided [47]. To get an in depth understanding of these experimental curves (Fig. 10a and c), a set of simulations are arranged to produce the transient curves.

In order to permit comparison of the calculated transient curves with the experiment [47], the same definition is used in our simulation, for relative activity, namely the ratio of the conversion at t (s) to that at 5 s. It should be noted that the time scale cannot be the same because we did not consider, in our reactor model, the hydrodynamic effects (hold-up, replacement, etc.) which existed in experiments. Starting from a zero surface concentration of spillover hydrogen, simulation results predict that both HYD and HDS activities always increase with time during the start up period. This was not always true in experimental observations [47]. By changing the initial values of the concentration of spillover hydrogen on the Acceptor (MoS_2) phase for different runs, which may reflect correctly a different influence of pretreatment on catalysts of different compositions, it is possible to simulate all the trends observed in experiments [47] as shown in Fig. 10b and d. It is clear from this simulation that the pretreatment of catalysts influences their activation behaviors significantly. The transient curves observed in experiments [47] do not arrange regularly in the order of increasing Co (promoter) content (increasing ρ). This may result from different extents of the accumulation of mobile hydrogen species on the catalyst surface because of the slightly different environment of the

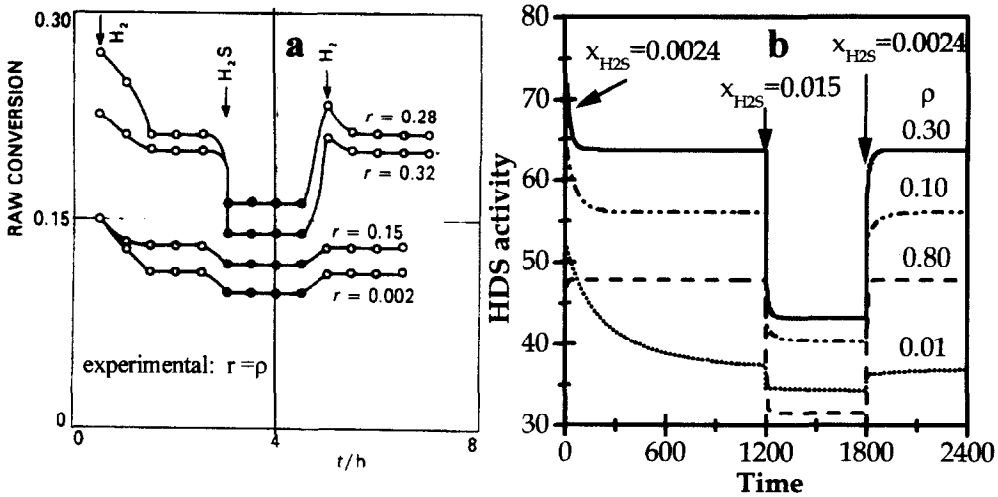

Fig. 11. Switch operation: the feed is switched between high H_2S concentration and low H_2S concentration, $P = 40$ bar.

pretreatment. Let us note also that the loss of activity observed in thiophene HDS for pure MoS_2 can also be correctly repeated by the model (experimental: Al–S–0.0 and simulation: Co/(Co + Mo) = 0.0 in Fig. 10). But the loss of activities over pure Co_9S_8 was not taken into account in the model because we neglected the activity of Co_9S_8. The experimental phenomena can be explained as the rapid deactivation of pure Co_9S_8 phase on stream.

The second case corresponds to switching between feeds with different H_2S concentrations. Corresponding experiments have been reported for atmospheric pressure tests [48]. The conditions used in the present work, however, correspond to more realistic HDS and HYD operation conditions with $P = 40$ bar and feed composition listed in Table 4. It is found that the variations of HDS activity are generally comparable to the experimentally observed ones (Fig. 11). The addition of H_2S depresses the HDS activity. The simulation results confirm the experimentally discovered striking phenomena [48] that, for catalysts with different compositions, the depression of activity is stronger when the synergy effect is stronger (catalysts in strong synergy range: $\rho = 0.3$, $\rho = 0.1$ for simulation) and weaker when synergy effect is weaker (catalysts in weak synergy range: $\rho = 0.01$ for simulation). It should be noticed however that the experimental synergy ranges are different: strong synergy ($\rho = 0.28$ and $\rho = 0.3$) and weak synergy ($\rho = 0.002$ and $\rho = 0.15$). The simulation result for large promoter proportion, $\rho = 0.8$, which does not correspond to experiments [48], shows that the addition of H_2S depresses substantially (almost completely) the HDS activity of catalysts with high ρ values (Fig. 11b).

The third case of transient behavior corresponds to the cases when the flow rate of the feed is changed. The operation conditions are those with high H_2S pressure as listed in Table 4. The initial time corresponds to that at which an empty reactor begins to be fed by the reaction mixture and the catalyst surface has not yet been contacted with hydrogen, namely the surface concentration of spillover hydrogen is 0. The simulation results show that, when the system starts with a low flow rate of liquid feed ($W_t/F_l = 5.0$ kg h/kmol), the HDS activity (conversion) stabilizes at a high value (Fig. 11). When the liquid feed is suddenly switched to a high flow rate ($W_t/F_l = 1.0$), the HDS activity diminishes sharply to reach a low level at first and later gradually increases to a slightly higher stable level (solid line). When the flow rate is suddenly switched back to the original value ($W_t/F_l = 5.0$), the HDS activity immediately changes back to a slightly higher level than the original steady state

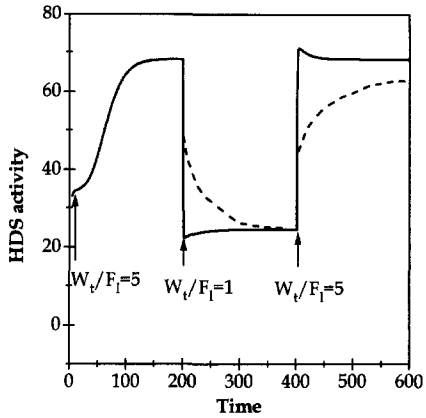

Fig. 12. Flow rate switch operation: $p = 0.3$, $P = 60$ bar.

value and then gradually declines to the original activity (solid line). Corresponding experiments were reported by Broderick et al. [49] for the HDS of dibenzothiophene (DBT) in a gas–liquid reaction system. However, due to the existence of strong hydrodynamic (hold up) effects in the reported experimental because of the coexistence of gas and liquid phases in the reactor, the experimental results showed a very long time-delay effect as qualitatively indicated by dashed lines in Fig. 12. The irreversible behavior the experiments indicated (dashed line in Fig. 12) might be ascribed to a bi-stability of the HYD and HDS system, as reported by the authors. This could be caused by the strong non-linearity of the kinetics of HDS and HYD reactions. However, we have not yet been able to reproduce in a self-consistent way this bi-stability with our model considering a pseudo-homogeneous system (gas phase). The irreversible behavior (schematically indicated in dashed lines in Fig. 12) observed in these experiments, namely the fact that the activity could not reach the same level as before the temporary change of flow rate, may be seriously influenced by the hydrodynamic (hold-up, stagnant volume, replacement, etc.) effects, which prevail in a gas–liquid system. A simple comparison between the time needed to stabilize after the first switch (space time switched from 123 units to 730 units: nearly 50 h for the system stabilization) and after the second switch and the two values of space time (123 and 730) used in the transient experiments of the above cited authors [49] leads to the conclusion that at least 300 h would be needed to stabilize their system after the second switch while their experiments lasted only 80 h. The conclusion here is again that specially designed experiments should be made to clarify this point, for example, transient experiments in a wide operation condition range on the basis of available data, especially the work commented above [49].

The contact quality between the two phases, namely the donor and the acceptor, is another important factor influencing the activity of the HDS and HYD reactions. In the frame of the remote control theory, Pirotte et al. designed an experiment, in which they modified the intimacy of contact, and measured the corresponding variations of HDS and HYD activity (and the HDS/HYD selectivity). For that they pressed a mixture of Co_9S_8 and MoS_2 at different pressures, thus minimizing the distance between particles, very likely increasing in this way the number and/or contact area of the mutual contacts [50]. The simulation results of the present work show that with the decrease in contact distance, namely with increasing compression pressure, the activity of HYD increases gently, but the HDS activity increases more rapidly than that of HYD. This qualitatively reproduces the experimental observations by Pirotte et al. [50] as shown in Fig. 13 (upper: experimental, down: simulated). However, for a quantitative correlation between the diffusion distance, L, defined in this work, and

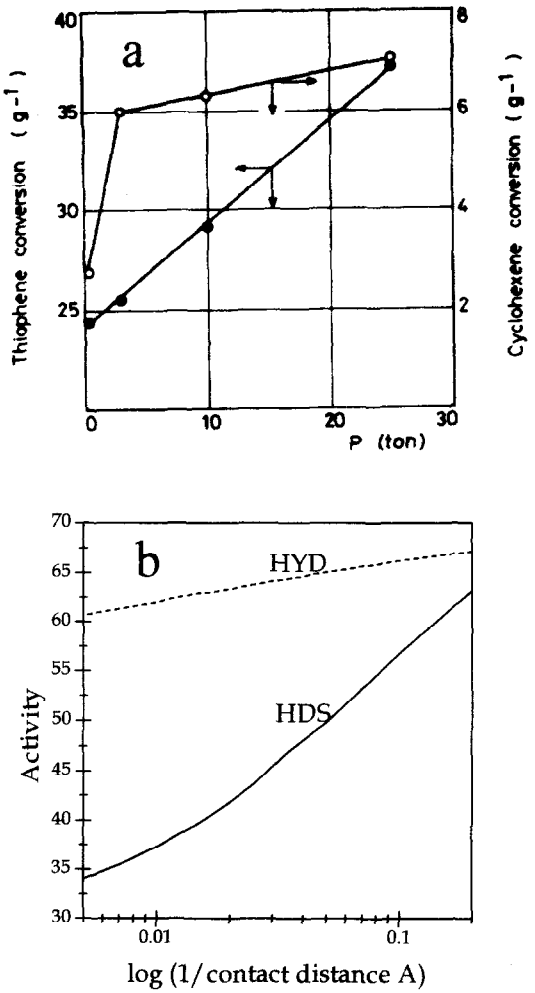

Fig. 13. Effect of the quality of contact on the activities of HYD and HDS. $p = 0.30$, $P = SO$ bar, feed in Table 4, high H_2S group.

activity, the correspondence between L and the compressing pressure used in the preparation of catalysts should be established on the basis of experimental measurements. These data are not yet available.

6. Conclusion

The remote control was combined with available representation of the surface structure and kinetic information on HYD and HDS reactions in order to analyze the real kinetics of these reactions. In the frame of the remote control theory, three possibilities of interconversion between HYD and HDS sites have been investigated comprehensively. These concern the atomic scale changes in the interconversion of HYD and HDS sites. These possibilities are: (1) model G: 3-fold CUS sites, HYD sites, are reduced to form 4-fold CUS sites for HDS, (2) model I: a bridging S atom between two vicinal HYD sites (3-fold CUS sites) is attacked by spillover hydrogen, $H_{so,Mo}$, to form one HDS site, which is constituted of two cooperation 3-fold-CUS metal sites, one to which an SH group is attached and the

other one carrying a hydrogen atom (proton) and (3) model J: a bridging S atom is attacked by H_2S, forming two HDS sites which are 3-fold CUS sites, each of which is bound with an SH group. It was found that model G and model I can correctly predict all observed chemical trends. The SH groups probably involved in HDS sites are not formed by H_2S adsorption and reaction because this mechanism (model J) leads to a wrong prediction of known chemical trends. The breaking of Mo–S bonds attached to HYD sites by spillover hydrogen, as assumed by both model G and model I, brings about the formation of HDS sites.

Simulation results show that the hypothesis of the remote control theory, namely the migration of spillover hydrogen from donor to acceptor, the creation of the active sites on the acceptor and the interconversion between HYD sites and HDS sites, is adequate to describe the observed experimental trends in HYD and HDS catalysis. This work suggests that detailed information on the catalyst surface and even on the structures of the active sites can be included in a kinetic model based on the remote control hypothesis. The consequence is that a comprehensive kinetic model, adequate to catalyst design purposes, could be obtained on the basis of the remote control model, provided systematic kinetics experiments are designed to reflect all the aspects of HYD and HDS catalysis, namely the synergy effect, the influence of H_2S, and all the other parameters determining the kinetics.

7. Notation

D_S	surface diffusivity of spillover hydrogen from donor to acceptor $D_S = D_{S,0}\exp(-E_S/R_gT)$ (m^2/s)
$D_{S,0}$	pre-exponential factor of the surface diffusivity of H_{so} (m^2/s)
E_S	activation energy of the migration of the spillover hydrogen on catalyst surface (J/mol)
F^0	volume flow rate of the reactant mixture at reactor inlet at P and T (m^3/s)
F	volume flow rate of the reactant mixtures at reactor outlet at P and T (m^3/s)
K_i, K^0	adsorption or chemical reaction equilibrium constant for step i, see Table 2 for units
k_i	rate constant for step i, see Table 2 for units
L	characteristic diffusion distance of spillover hydrogen, m
$[Mo]_t$	total concentration of metal sites on the edges of MoS_2, which have to be activated by spillover hydrogen (mol/m^2 Mo)
$[Mo]_t^0$	total concentration of metal sites on the edges of MoS_2, which exist in the originally defective structure (mol/m^2 Mo)
P	total pressure (bar)
P_i	partial pressure of component i, i = T, S, H_2, H_2S, B and A (bar)
R_g	gas constant (8.314 J/mol K)
r_i	reaction rates (mol/s m^2 Mo)
r_c	rate of the loss of spillover hydrogen on Acceptor (mol/s m^2 Mo)
S_{Co}	specific surface area of Co_9S_8 phase (m^2/mol Co)
S_g	specific surface area of catalyst (m^2/kg cat)
S_{Mo}	specific surface area of MoS_2 phase (m^2/mol Co)
T	temperature (K)
V_R	reactor volume (m^3)
X_{HDS}	conversion of thiophene defined in Eq. (35)
X_{HYD}	conversion of unsaturated hydrocarbons defined in Eq. (36)

x_i mole fraction of component i in reaction mixtures in the reactor and at the outlet of the reactor
x_i^0 mole fraction of component i in feed
$[^*]$ surface concentration of intermediate species or sites (mol/m^2 active phase)

Greek symbols

β mol number of (Co + Mo) in 1 kg catalyst
ε_B specific free space of the catalyst bed
π edge Mo sites (2 fold CUS sites)
ρ proportion of promoter represented by Co/(Co + Mo) (mol ratio)
ρ_{cat} apparent density of catalyst particles used in reactor, kg/m^3
σ HDS sites created during reaction
σ^0 HDS sites originally formed during preparation and pretreatment stage
τ HYD sites created during reaction
τ^0 HYD sites originally formed during preparation and pretreatment stage

Subscripts

T thiophene
S solvent
B unsaturated hydrocarbons
A paraffins
R reactor

Acknowledgements

Financial support from the Services Fédéraux des Affaires Scientifiques, Techniques et Culturelles (Belgium) and Unité de catalyse et Chimie des Matériaux Divisés (CATA), Université Catholique de Louvain is greatly acknowledged (Y.-W.L.). We are grateful to many interesting discussions with Professor P. Grange, Dr. P. Ruiz (Unité CATA), Dr. X. Gonze and Dr. J-C. Charlier (Unité PCPM, UCL) in the progress of this work. We appreciate the discussions on experimental aspects of hydrotreating catalysis with Mr. M.-H. Yang and Mr. R. de Back in Unité CATA.

References

[1] B. Delmon, in: D.L. Trimm, S. Akashah, M. Absi-Halabi, A. Bishara (Eds.), Catalysts in Petroleum Refining 1989, Elsevier, Amsterdam, 1990, pp. 1–40.
[2] R.C. Pille, C.-Y. Yu, G.F. Froment, J. Mol. Catal. 94 (1994) 369.
[3] M. Yamada, K. Kawahara, S. Kasahara, Proc. of First Joint Workshop on the Frontiers of Catalytic Science and Technology (JECAT '91), 1991, p. 2.
[4] M. Yamada, T. Obara, J.W. Yan, S. Hatakeyama, Sekiyu Gakkaishi 31 (1988) 118.
[5] M. Yamada, T. Obara, J.W. Yan, S. Hatakeyama, CA 108 (1988) 170383t.
[6] B. Delmon, Bull. Soc. Chim. Belg. 104 (1995) 173.
[7] B. Delmon, G.F. Froment, Catal. Rev. Sci. Eng. 38 (1996) 69.
[8] H. Topsøe, B.S. Clausen, F.E. Massoth, in: J.R. Anderson, M. Boudart (Eds.), Hydrotreating Catalysis, Springer, Berlin, 1996.
[9] I.A. Van Parijs, G.F. Froment, Chem. Eng. Sci. 25 (1986) 431.
[10] I.A. Van Parijs, G.F. Froment, Appl. Catal. 21 (1986) 273.
[11] G. Villora, A.O. Beyne, G.F. Froment, Ind. J. Technol. 29 (1991) 128.

[12] C.-Y. Yu, G.F. Froment, Chem. Eng. Sci. 46 (1991) 3177.
[13] T. Rebitzki, B. Delmon, J.H. Block, AIChE J. 41 (1995) 1543.
[14] S. Kasztelan, J. Jalowiecki, A. Wambeke, J. Grimblot, J.P. Bonnelle, Bull. Soc. Chim. Belg. 96 (1987) 1003.
[15] S. Kasztelan, H. Toulhoat, J. Grimblot, J.P. Bonnelle, Appl. Catal. 13 (1984) 127.
[16] Y. Okamoto, H. Tomioka, Y. Katoh, T. Imanaka, S. Teranishi, J. Phys. Chem. 84 (1980) 1833.
[17] Y. Okamoto, H. Tomioka, T. Imanaka, S. Teranishi, J. Catal. 66 (1980) 93.
[18] F.E. Massoth, C.L. Kibby, J. Catal. 47 (1977) 300.
[19] J. Bachelier, M.J. Tilliette, J.C. Duchet, D. Cornet, J. Catal. 76 (1982) 300.
[20] J. Bachelier, J.C. Duchet, D. Cornet, J. Catal. 87 (1984) 283.
[21] J. Bachelier, M.J. Tilliette, J.C. Duchet, D. Cornet, J. Catal. 87 (1982) 292.
[22] S. Eijsbouts, J.J.L. Heinerman, Appl. Catal. A 105 (1993) 53.
[23] S. Eijsbouts, J.J.L. Heinerman, Appl. Catal. A 105 (1993) 69.
[24] R. Prins, V.H.J. De Beer, G.A. Somorjai, Catal. Rev. Sci. Eng. 31 (1989) 1.
[25] M. Daage, R.R. Chianelli, J. Catal. 149 (1994) 414.
[26] A.N. Startsev, Catal. Rev. Sci. Eng. 37 (1995) 353.
[27] C.J. Wright, C. Sampson, D. Fraser, R.B. Moyes, P.B. Wells, J. Chem. Soc. Faraday Trans. I 76 (1980) 1585.
[28] J. Materova, Appl. Catal. 3 (1982) 3.
[29] F.E. Massoth, P. Zeuthen, J. Catal. 145 (1990) 216.
[30] S.Y. Li, J.A. Rodriguez, J. Hrbek, H.H. Huang, G.-Q. Xu, Surf. Sci. 366 (1996) 29.
[31] R.R. Chianelli, M. Daage, M.J. Ledoux, Adv. Catal. 40 (1994) 177.
[32] O. Weisser, S. Landa, Sulfide Catalysts: Their Properties and Applications, Pergmon, Oxford, 1973.
[33] A.F. Wells, Structural Inorganic Chemistry, 5th ed., Oxford University Press, New York, 1987.
[34] Yu.I. Yermakov, A.N. Startsev, V.A. Burmistrov, O.N. Shumilo, N.N. Bulgakov, Appl Catal. 18 (1985) 33.
[35] B. Delmon, Surf. Rev. Lett. 2 (1995) 25.
[36] B. Delmon, J.-L. Dallons, Bull. Soc. Chim. Belg. 97 (1988) 473.
[37] G.C. Hadjiloizou, J.B. Butt, J.S. Dranoff, Ind. Eng. Chem. Res. 31 (1992) 2503.
[38] B. Delmon, Bull. Soc. Chim. Belg. 88 (1979) 979.
[39] D. Pirotte, P. Grange, B. Delmon, in: T. Seiyama, K. Tanabe (Eds.), Proc. 7th Int. Congress Catalysis, Elsevier, 1981, pp. 1422–1423.
[40] R. Kramer, M. Andre, J. Catal. 58 (1979) 287.
[41] C.N. Satterfield, G.W. Roberts, AIChE J. 14 (1968) 159.
[42] J.M. Asua, B. Delmon, Ind. Eng. Chem. Res. 26 (1987) 32.
[43] J.M. Asua, B. Delmon, Appl. Catal. 12 (1984) 249.
[44] J. van Gestel, L. Finot, J. Leglise, J.C. Duchet, Bull. Soc. Chim. Belg. 104 (1995) 189.
[45] D.H. Broderick, B.C. Gates, AIChE J. 27 (1981) 663.
[46] N. Marchal, S. Mignard, S. Kasztelan, Catal. Today 29 (1996) 203.
[47] P. Gajardo, A. Mathieux, P. Grange, B. Delmon, Appl. Catal. 3 (1982) 347.
[48] B. Delmon, in: H.F. Barry, P.C.H. Mitchell (Eds.), Chemistry and Uses of Molybdenum, Climax Molybdenum Company, Ann Arbor, Michigan, 1979, pp. 73–84.
[49] D.H. Broderick, G.C.A. Schuit, G.C. Gates, J. Catal. 54 (1978) 94.
[50] D. Pirotte, J.M. Zabala, P. Grange, B. Delmon, Bull. Soc. Chim. Belg. 90 (1981) 1239.